CEA Comité Español de Automática
XLVI JORNADAS AUTOMÁTICA CARTAGENA 2025
UNIVERSIDADE DA CORUÑA

Jornadas de Automática

Embedded Flex Sensor for Posture Estimation and Control of a Soft Robotic Neck

Miglietta, Gianluca[a,*], Sánchez, Claudia[b], Muñoz, Jorge[b], Martínez, Santiago[b], Monje, Concepción A.[b]

[a] *Dipartimento di Elettronica, Informazione e Bioingegneria (DEIB). Politecnico di Milano, Piazza Leonardo da Vinci 32, 20133 Milano, Italy.*
[b] *Department of Systems Engineering and Automation, RoboticsLab, Carlos III University of Madrid, Av. de la Universidad, 30, 28911 Leganés, Madrid, Spain.*

To cite this article: Miglietta, G. Sánchez, C. Muñoz, J. Martínez, S. Monje, C. A. 2025. Embedded Flex Sensor for Posture Estimation and Control of a Soft Robotic Neck. Jornadas de Automática, 46. https://doi.org/10.17979/ja-cea.2025.46.12225

Abstract

This work presents a soft robotic neck with embedded sensing for posture estimation and control. A piezoresistive strain sensor, 3D-printed using TPU and carbon black, is integrated into the soft link to measure bending directly. The sensor's resistance is mapped to pitch angle through third-order polynomial models, fitted separately for loading and unloading phases to capture hysteresis. A switching strategy based on signal slope dynamically selects between models for real-time estimation. For control, a fractional-order PI (FOPI) controller is implemented, operating on the estimated pitch from the sensor. Despite a low sampling rate (2 Hz) and nonlinear sensor response, the system demonstrates stable closed-loop tracking of a sinusoidal reference trajectory. Experimental results confirm that embedded sensing allows autonomous neck movement without relying on external IMUs. The approach offers a low-cost, compact solution for integrating sensing and control in soft robots. This work supports the development of self-contained, bioinspired robotic systems with enhanced autonomy and adaptability.

Keywords: Soft robotics, Posture estimation, Embedded sensing, Fractional-order control

Sensor flexible embebido para la estimación postural y control de un cuello robótico blando

Resumen

Este trabajo presenta un cuello robótico blando con un sensor embebido para la estimación y control de su postura. Un sensor piezorresistivo, impreso en 3D con TPU y negro de carbono, se integra en el cuerpo del cuello para medir directamente la curvatura. La resistencia del sensor se convierte en ángulo de pitch mediante modelos polinómicos de tercer orden, ajustados por separado para las fases de carga y descarga, capturando la histéresis. Para la estimación en tiempo real, se emplea una estrategia de conmutación basada en la pendiente de la señal. El control se realiza mediante un controlador PI de orden fraccionario (FOPI), que opera sobre el ángulo estimado sin necesidad de sensores externos. A pesar de la baja frecuencia de muestreo (2 Hz) y del comportamiento no lineal del sensor, el sistema logra un seguimiento estable de una trayectoria sinusoidal de referencia. Los resultados validan el uso de sensado embebido como alternativa compacta y de bajo coste, orientada al desarrollo de sistemas robóticos blandos autónomos y bioinspirados.

Palabras clave: Robótica blanda, Estimación postural, Sensado embebido, Control de orden fraccionario

1. Introduction

Unlike traditional rigid robots, soft robots have rapidly gained attention as a transformative approach in the robotic field. They offer intrinsic compliance, adaptability, and safety in environments where conventional rigid robots may pose risks or limitations (Iida and Laschi, 2011; Yasa et al., 2023). These characteristics make soft robots a suitable option for applications involving robot-human interaction (Polygerinos et al., 2017), medical devices (Cianchetti et al., 2018), or manipulation (Shintake et al., 2018).

*Autor para correspondencia: clausanc@ing.uc3m.es

Bioinspiration is a key design principle in this field, where the morphology and function of soft systems aim to mimic those of biological organisms. This strategy enables the development of robots capable of bending, twisting, extending, and flexing using compliant materials and simple, low-cost actuation mechanisms. However, reproducing biological systems' structural and functional complexity often leads to soft robots with bodies that undergo large, nonlinear deformations, which challenge conventional methods of control and sensing (Ahmed et al., 2022; Roche et al., 2014). Although significant advances have been made in soft material sensing technologies, integrating sensors and control systems remains challenging. Traditional sensing methods, such as inertial measurement units (IMU) and external vision systems, are designed for rigid body motion and often fail to capture the complex deformation of soft structures with sufficient accuracy. Moreover, in many cases, the end effector is neither free nor directly visible, which restricts the use of external tracking systems. As a result, there is a growing need for fully integrated, embedded sensing solutions tailored to the unique requirements of soft robots, along with control strategies that rely directly on feedback from these embedded sensors rather than external sources.

Several researchers have explored the integration of sensors into soft robotic structures to enable deformation monitoring and closed-loop control. Gerboni et al. integrated commercial flex bend sensors into flexible fluid actuators to enable closed-loop control of soft bending modules. The sensors measured single-axis curvature, and an onboard microcontroller processed their signals. A proportional-integral controller was implemented, achieving tip positioning with less than 1 mm error, demonstrating accurate and low-cost feedback control in soft robotics (Gerboni et al., 2017). Similarly, Elgeneidy et al. used a data-driven approach to control the bending angle of a soft pneumatic actuator embedded with a resistive flex sensor. Sensor feedback was synchronized with visual measurements to train empirical models using regression and neural networks. These models were then used in a PID controller to track reference signals under varying conditions, showing that data-driven methods can effectively control soft actuators without requiring complex physical modeling (Elgeneidy et al., 2018). In another approach, Ji et al. demonstrated closed-loop shape control of soft actuators using 3D-printed resistive sensors made from commercially available soft conductive material. Various sensor configurations were tested, with the optimal design providing accurate shape estimation through resistance changes. Compared to commercial bending sensors, the printed sensor had lower stiffness and better integration, enabling precise control without degrading actuator performance. The approach was validated on a soft gripper with individually controlled fingers (Ji et al., 2023).

These works highlight the potential of combining embedded strain sensing with simple control strategies to improve actuation accuracy in soft systems. Motivated by these promising results, we explore a similar sensing approach in a different morphological platform, a bioinspired soft robotic neck. Our system uses a 3D-printed strain sensor made from thermoplastic polyurethane (TPU) and carbon black (CB), manually embedded into the structure. This sensor provides direct curvature feedback that is used to close the control loop of the neck's tilt, aiming to replicate realistic bending behavior without relying on external tracking systems.

2. Soft robotic neck

The soft robotic neck (Figure 1a-c) is a bioinspired structure that emulates the flexibility and compliance of the human cervical spine. It is actuated by a cable-driven parallel mechanism (CDPM) composed of three tendons arranged with 120° separation around a deformable central body. Each tendon is independently actuated by a servomotor to induce coordinated bending motions in the structure, enabling multi-directional tilt and orientation of the upper platform (Muñoz et al., 2024, 2020; Mena et al., 2020).

In previous work, a 3D-printed piezoresistive strain sensor composed of two layers of TPU and a CB matrix with a silver ink interdigitated electrode (IDE) between them was embedded within the internal cylindrical channel of the soft link. While this configuration successfully demonstrated the sensor's capability to detect joint curvature, the rectangular geometry of the sensor was not well suited to the circular internal structure of the link. This geometric mismatch introduced limitations in accurately capturing the deformation associated with the neck's natural bending modes. Specifically, the circular placement resulted in non-uniform strain distributions, making it difficult to establish a consistent and meaningful relationship between the sensor's electrical output and the actual posture of the system (Sanchez et al., 2025).

To address these limitations, the structure was redesigned around a central spine-like geometry using thermoplastic elastomer (TPE) as the core material. The new link features a straight, longitudinal channel passing through the center of the soft body, allowing for the manual insertion of the strain sensor along the primary bending axis. This modification, depicted in Figure 1d-f, results in a more direct mapping between the sensor's resistance change and the curvature of the neck, significantly improving sensing linearity and repeatability.

Additionally, the sensor's central alignment ensures a symmetric response to bidirectional bending and avoids the cross-sensitivities and mechanical offsets observed in the earlier radial configuration. The parallel actuation mechanism remains unchanged, preserving the muscular analogy, but the improved structural and sensing design enables more accurate reproduction of continuous, smooth head-like motions.

This updated configuration enhances posture estimation accuracy and facilitates embedded sensing in scenarios where external measurement tools such as IMUs become impractical. By aligning the sensor with the central deformation axis and integrating it seamlessly into the new structural layout, the system achieves better coherence between actuation, deformation, and measurement, an essential step toward robust, fully embedded soft robotic control.

3. Embedded sensor calibration

The embedded strain sensor is calibrated to establish a reliable mapping between its electrical resistance and the pitch angle of the soft robotic neck.

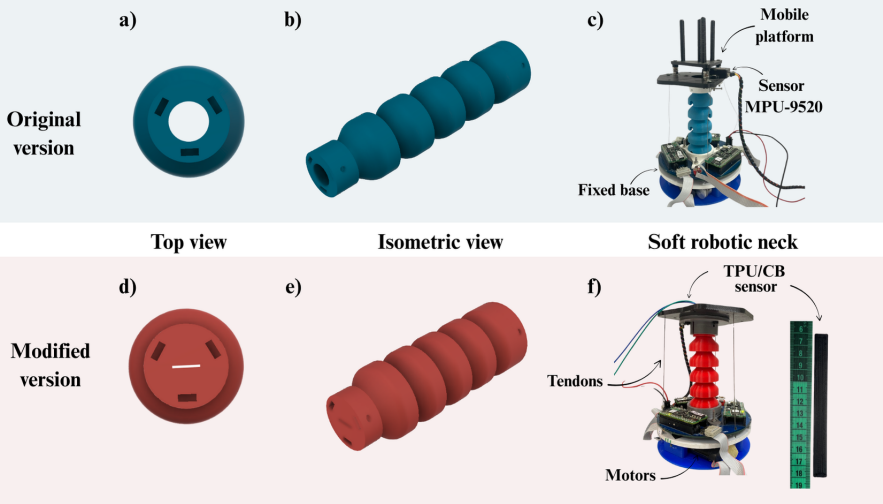

Figure 1: Comparison between the original (a–c) and modified (d–f) versions of the soft robotic neck. The original design uses a soft link with tendon channels and an external IMU (MPU-9250) for posture estimation. The modified version introduces a central channel to embed a TPU/CB strain sensor, enabling internal sensing. Both versions preserve the tendon-driven actuation with three motors and a mobile platform.

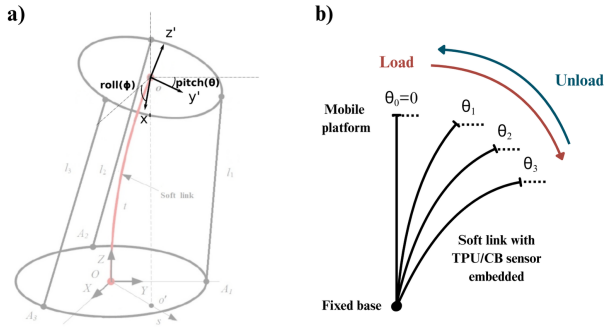

Figure 2: (a) Soft neck coordinate frame showing pitch and roll rotations (Muñoz et al., 2024). (b) Bending trajectories during load and unload phases with embedded TPU/CB strain sensor.

The neck bends in smooth, planar motion under tendon actuation, producing pitch variations $(\theta_0, \theta_1, \theta_2, ...)$ during loading and unloading cycles (Figure 2). These quasi-static tests are limited to a small strain range to remain within the sensor's linear response. After discarding initial cycles to allow stabilization, a reference resistance R_0 is defined, and the normalized resistance change is computed as:

$$\Delta R = \frac{R_{\text{flex}} - R_0}{R_0} \tag{1}$$

A data-driven piecewise model maps ΔR to pitch angle θ, with separate fits for load and unload segments. Due to the viscoelastic nature of the materials, hysteresis occurs between the curves. To reduce its impact, an average model is also computed and used when a single curve is preferred.

To improve estimation during real-time operation, a switching strategy selects between the load and unload models based on the slope of the resistance:

$$\text{slope} = \frac{\Delta R_{\text{curr}} - \Delta R_{\text{prev}}}{t_{\text{curr}} - t_{\text{prev}}} \tag{2}$$

For smoother transitions, a sigmoid function is used:

$$\text{sigmoid} = \frac{1}{1 + e^{-\alpha \cdot \text{slope}}} \tag{3}$$

This combines the two models based on the slope's sign and magnitude. A high α approximates a hard switch; a low α behaves more like the average model.

The sensor is aligned along the central bending axis of the soft link, ensuring a more homogeneous strain distribution and improved signal quality. This configuration enhances linearity and repeatability, critical features for accurate posture estimation and closed-loop control.

4. Control strategy

The control objective is to regulate the pitch angle θ of the soft robotic neck so that it tracks a desired reference trajectory θ_{ref}. Given the inherent compliance and nonlinear behavior of soft materials, along with the low sampling rate imposed by the resistance acquisition system (2Hz), a robust control approach is required.

Figure 3 illustrates the closed-loop control architecture implemented in this work. The resulting error signal e_θ is processed by a controller that generates a command in velocity to actuate the motors driving the tendons. Similar to previously IMU-based feedback schemes in earlier versions of the system, a fractional robust control scheme was selected for its robustness and smooth dynamic response in systems with limited bandwidth and nonlinear dynamics, such as soft actuators. Given the sensor's measurement problems discussed before, an accurate plant model was not possible, and a model-based controller tuning was discarded. Instead, an experimental tuning procedure was used. Starting from a known integer order PI controller, the exponent was found by trial and error, seeking to obtain a smooth response, robust to changes in the neck position, resulting in a fractional-order PI (FOPI) controller, defined by the following transfer function:

$$FOPI(s) = 0.6443 + 3.2325 s^{-0.85} \tag{4}$$

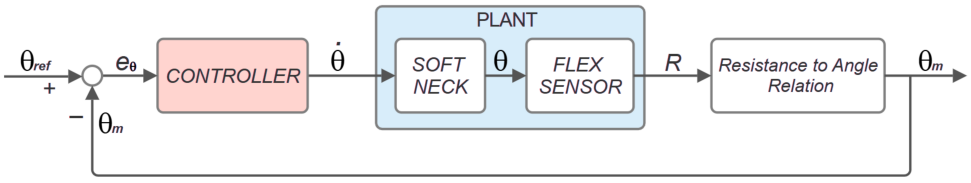

Figure 3: Closed loop scheme, applied to the neck's position control. Transducer block converts measured resistance to pitch angle.

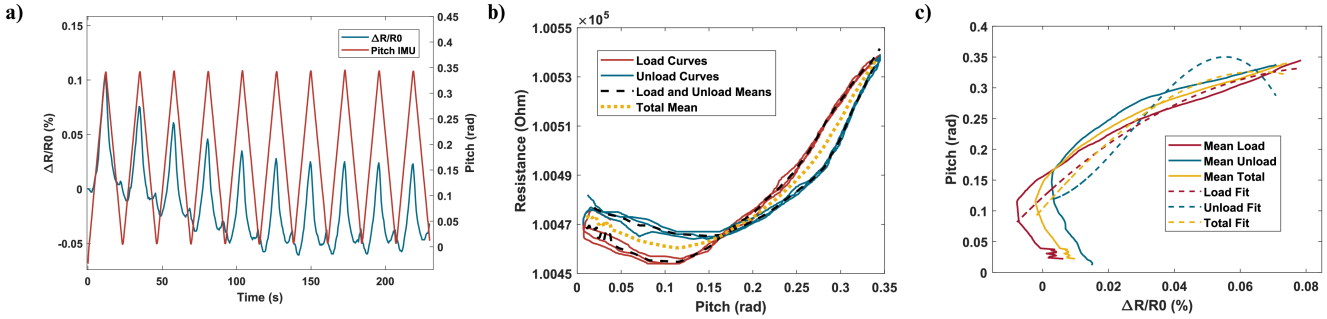

Figure 4: Sensor calibration and model fitting. a) Time evolution of resistance variation and IMU-measured pitch during cyclic bending. b) Static resistance–pitch mapping. c) Fitted polynomial models for pitch estimation from normalized resistance data.

This controller formulation balances proportional and memory-based (fractional integral) actions, which is particularly suitable for systems with low sensor update rates and time-dependent material behaviors. Overall, the control strategy emphasizes practicality and robustness in the face of sensor nonlinearity, sampling limitations, and soft material dynamics. By leveraging a fractional-order design and embedding the sensor directly in the structure, the system achieves closed-loop control of posture with minimal external instrumentation, aligning with the broader goal of developing self-contained soft robotic platforms.

5. Experimental results

5.1. Embbeded sensor modeling

The embedded strain sensor was evaluated over repeated bending cycles to assess its ability to estimate neck pitch. As shown in Figure 4a, after a few cycles of initial drift, the resistance signal stabilizes and begins to follow the IMU-measured pitch trend, confirming the need for a preload phase before reliable use in closed-loop control. However, during transitions from negative to positive pitch slopes, particularly near the vertical position, secondary resistance peaks emerge. These artifacts, clearly visible in the 0–0.1 rad range in Figure 4b, introduce a local inverse proportionality between pitch and resistance, leading to non-monotonic behavior and poor fitting accuracy in that region. To capture these nonlinear and asymmetric trends, three separate third-order polynomial models were fitted as depicted in Figure 4c: one for the loading phase, one for the unloading phase, and one averaged model representing the overall trend. Each model follows the general form:

$$R(\theta) = a\theta^3 + b\theta^2 + c\theta + d \tag{5}$$

where $R(\theta)$ denotes the resistance as a function of pitch angle θ. The fitted coefficients a,b,c, and d, along with the coefficient of determination (R^2) for each model, are summarized in Table 1. These values quantitatively reflect the models' ability to reproduce the experimental mapping.

Table 1: Third-order polynomial coefficients for the static resistance–pitch mapping during load, unload, and total phases.

Model	a	b	c	d	R^2
Total	-1.81×10^8	-2.84×10^5	603.33	0.10	0.85
Load	-2.67×10^9	2.19×10^6	26.63	0.12	0.59
Unload	-2.21×10^7	-3.04×10^5	492.46	0.12	0.78

Figure 5 presents the validation of the total and switching models against the IMU pitch signal. During the initial cycles of validation, pitch estimates deviate significantly, by up to 1000%, due to early instability in the resistance response. This further reinforces the necessity of performing a stabilization phase before engaging the model in control. As highlighted in the zoomed inset, both models perform well in the 0.1–0.35 rad range, but deviate near 0 rad due to secondary resistance peaks. These artifacts result in local overestimation of pitch during direction changes. Overall, the switching model yields better agreement than the total model, especially during asymmetric transitions, confirming the advantage of slope-aware modeling for embedded posture estimation. To address the resistance peak problem, signal filtering was explored. A low-pass filter removes secondary peaks but also attenuates true curvature, degrading accuracy during transitions. A reference-based filter was also considered but discarded, as real-time pitch cannot be assumed to match the reference due to actuation delays and external disturbances.

5.2. Closed-loop control performance

The final validation phase focused on assessing whether the embedded strain sensor and calibrated curvature model could support real-time closed-loop control of the soft robotic neck. The objective was to follow a sinusoidal pitch trajectory using only strain-based feedback, without relying on external measurements such as IMUs.

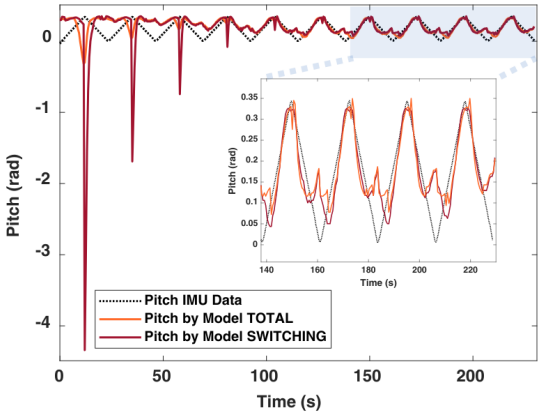

Figure 5: Comparison of pitch estimates from total and switching models against IMU data. Inset shows detail during steady oscillations.

The control strategy was implemented using the fractional-order PI (FOPI) controller introduced earlier. Due to hardware limitations, sensor readings were acquired at 2 Hz via a benchtop multimeter. To account for this low sampling rate and prevent instability, the controller gains were scaled accordingly. Before each test, the system underwent an open-loop preload phase to bring the neck to a neutral position and stabilize the sensor's baseline resistance. Figure 6 illustrates the difference between raw and filtered pitch estimates. While a second-order Butterworth filter (cutoff = 5 Hz) was effective in reducing high-frequency noise, it also introduced undesirable delay and attenuated curvature peaks. This filtering impaired the sensor's responsiveness during directional changes, making it unsuitable for real-time control. As a result, the controller operated on the unfiltered strain-based signal. The core closed-loop result is shown in Figure 7. The neck was commanded to follow a slow sinusoidal reference pitch trajectory. The first two motion cycles were executed in open-loop, allowing the sensor to stabilize and defining a reliable baseline. The third cycle (shaded in red) was performed in closed-loop, with motor commands generated directly from the pitch estimate derived from the embedded strain sensor. During this closed-loop phase, the controller successfully shaped the neck's motion to follow the general form and timing of the reference signal. However, a pronounced amplitude mismatch is observed. The estimated pitch angle reaches a peak of approximately 0.68 rad, whereas the actual deflection measured by the IMU is only about 0.19 rad.

This overestimation leads the controller to produce stronger actuation than necessary, which paradoxically causes the physical motion of the neck to undershoot the intended target. This distortion stems from a combination of factors. First, the nonlinear strain-to-angle relationship causes the sensor model to amplify pitch values in regions with lower sensitivity or unmodeled saturation. Second, dynamic effects such as viscoelastic hysteresis and time-dependent rearrangement in the carbon-black network introduce additional error. These effects are not captured by the quasi-static calibration model used in the controller. Third, the low update frequency limits the controller's ability to react precisely to curvature changes, especially during acceleration and deceleration phases of the sinusoidal motion.

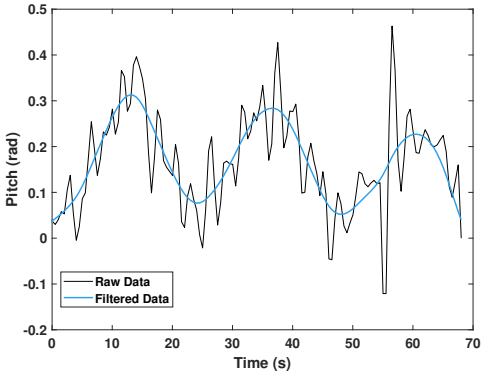

Figure 6: Raw and filtered pitch data showing noise reduction and smoothing of secondary peaks.

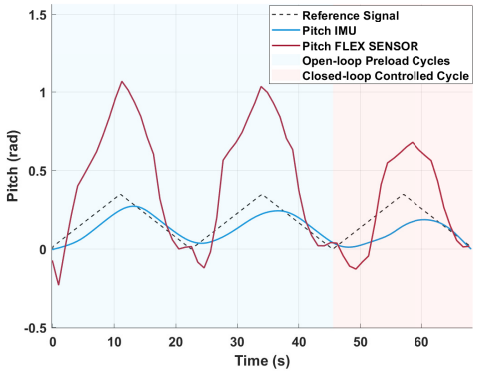

Figure 7: Closed-loop pitch tracking using the embedded flex sensor. Shaded regions indicate open-loop preload (blue) and closed-loop control (red).

Despite these challenges, the control system remained stable throughout the test. No oscillations or overshooting occurred, and the overall motion was smooth. This is partly due to the intrinsic mechanical compliance of the soft structure, which acts as a passive low-pass filter and helps absorb minor overcorrections. The robustness of the FOPI controller to model error and sampling delay also played a critical role in maintaining control quality.

The performance of the closed-loop system was evaluated by comparing the estimated pitch with the reference signal. The root-mean-square error (RMSE) over the third cycle was 0.2299 rad, and the maximum absolute error reached 0.3887 rad. These values are consistent with the previously observed calibration limitations and validate the system's ability to operate effectively in low-speed, low-precision tasks such as head orientation or gaze stabilization in soft robotic platforms.

In summary, the experiment demonstrates that a single embedded strain sensor, combined with a basic curvature model and a tuned FOPI controller, can enable posture control in a soft robotic system. While absolute accuracy remains limited by nonlinear sensor behavior and low sampling bandwidth, the approach eliminates the need for external measurement systems and supports future development of fully self-contained soft robotic platforms.

6. Conclusions

This work demonstrates the feasibility of closed-loop posture control in a soft robotic neck using a single embedded strain sensor and a slope-aware estimation model. A piezoresistive TPU/CB sensor was aligned along the central bending axis of the neck to maximize sensitivity and repeatability. By fitting third-order polynomial models to load and unload phases, the system captured key hysteretic effects, and a switching strategy based on resistance slope improved estimation near transition zones. The embedded signal was used directly in a fractional-order PI (FOPI) controller without external tracking. Despite constraints imposed by a 2 Hz sampling rate and model nonlinearities, the controller achieved smooth tracking with a root-mean-square error of 0.3887 rad. The experimental validation confirms the potential of low-cost, embedded sensing for posture control in soft robotic platforms. While limitations remain in absolute accuracy, the results support further exploration of fully integrated, sensor-based architectures in compliant robotics. This approach is especially promising for wearable or assistive applications where external instrumentation is impractical or undesirable.

Acknowledgments

The research leading to these results has been partially funded by the project SIROCO, with reference PID2023-147343OB-I00, funded by MICIU /AEI/10.13039/501100011033 and FEDER, UE, and the ADAPTA project, reference PLEC2023-010218, funded by MCIN/AEI/10.13039/501100011033.

References

Ahmed, F., Waqas, M., Jawed, B., Soomro, A. M., Kumar, S., Hina, A., Khan, U., Kim, K. H., Choi, K. H., Jun. 2022. Decade of bio-inspired soft robots: a review. Smart Materials and Structures 31 (7), 073002, publisher: IOP Publishing.
URL: https://dx.doi.org/10.1088/1361-665X/ac6e15
DOI: 10.1088/1361-665X/ac6e15

Cianchetti, M., Laschi, C., Menciassi, A., Dario, P., Jun. 2018. Biomedical applications of soft robotics. Nature Reviews Materials 3 (6), 143–153, publisher: Nature Publishing Group.
URL: https://www.nature.com/articles/s41578-018-0022-y
DOI: 10.1038/s41578-018-0022-y

Elgeneidy, K., Lohse, N., Jackson, M., Apr. 2018. Bending angle prediction and control of soft pneumatic actuators with embedded flex sensors – A data-driven approach. Mechatronics 50, 234–247.
URL: https://www.sciencedirect.com/science/article/pii/S0957415817301496
DOI: 10.1016/j.mechatronics.2017.10.005

Gerboni, G., Diodato, A., Ciuti, G., Cianchetti, M., Menciassi, A., Aug. 2017. Feedback Control of Soft Robot Actuators via Commercial Flex Bend Sensors. IEEE/ASME Transactions on Mechatronics 22 (4), 1881–1888, conference Name: IEEE/ASME Transactions on Mechatronics.
URL: https://ieeexplore.ieee.org/abstract/document/7914755?casa_token=xIwKRUIv4q4AAAAA:y1oDGWemog5V4adzwNQmzErkklnBav9flfGR7VtTwxOaHUE_PTgao1Y2ZhtnZ88KEkA6M9vpy0M
DOI: 10.1109/TMECH.2017.2699677

Iida, F., Laschi, C., Jan. 2011. Soft Robotics: Challenges and Perspectives. Procedia Computer Science 7, 99–102.
URL: https://www.sciencedirect.com/science/article/pii/S1877050911006958
DOI: 10.1016/j.procs.2011.12.030

Ji, Q., Jansson, J., Sjöberg, M., Wang, X. V., Wang, L., Feng, L., Jun. 2023. Design and calibration of 3D printed soft deformation sensors for soft actuator control. Mechatronics 92, 102980.
URL: https://www.sciencedirect.com/science/article/pii/S0957415823000363
DOI: 10.1016/j.mechatronics.2023.102980

Mena, L., Monje, C. A., Nagua, L., Muñoz, J., Balaguer, C., Mar. 2020. Test Bench for Evaluation of a Soft Robotic Link. Frontiers in Robotics and AI 7, publisher: Frontiers Media S.A.
DOI: 10.3389/frobt.2020.00027

Muñoz, J., Copaci, D. S., Monje, C. A., Blanco, D., Balaguer, C., 2020. Iso-m Based Adaptive Fractional Order Control With Application to a Soft Robotic Neck. IEEE Access 8, 198964–198976, conference Name: IEEE Access.
URL: https://ieeexplore.ieee.org/abstract/document/9247181
DOI: 10.1109/ACCESS.2020.3035450

Muñoz, J., de Santos-Rico, R., Mena, L., Monje, C. A., Apr. 2024. Humanoid Head Camera Stabilization Using a Soft Robotic Neck and a Robust Fractional Order Controller. Biomimetics 9 (4), publisher: Multidisciplinary Digital Publishing Institute (MDPI).
DOI: 10.3390/biomimetics9040219

Polygerinos, P., Correll, N., Morin, S. A., Mosadegh, B., Onal, C. D., Petersen, K., Cianchetti, M., Tolley, M. T., Shepherd, R. F., 2017. Soft Robotics: Review of Fluid-Driven Intrinsically Soft Devices; Manufacturing, Sensing, Control, and Applications in Human-Robot Interaction. Advanced Engineering Materials 19 (12), 1700016, _eprint: https://onlinelibrary.wiley.com/doi/pdf/10.1002/adem.201700016.
URL: https://onlinelibrary.wiley.com/doi/abs/10.1002/adem.201700016
DOI: 10.1002/adem.201700016

Roche, E. T., Wohlfarth, R., Overvelde, J. T. B., Vasilyev, N. V., Pigula, F. A., Mooney, D. J., Bertoldi, K., Walsh, C. J., Feb. 2014. A Bioinspired Soft Actuated Material. Advanced Materials 26 (8), 1200–1206.
URL: https://onlinelibrary.wiley.com/doi/10.1002/adma.201304018
DOI: 10.1002/adma.201304018

Sanchez, C., Rodrıguez, D., Otero, S., Monje, C. A., Jan. 2025. A Piezoresistive Printable Strain Sensor for Monitoring and Control of Soft Robotic Links. In: 2025 IEEE International Conference on Robotics and Automation (ICRA).
DOI: Accepted for publication

Shintake, J., Cacucciolo, V., Floreano, D., Shea, H., 2018. Soft Robotic Grippers. Advanced Materials 30 (29), 1707035, _eprint: https://onlinelibrary.wiley.com/doi/pdf/10.1002/adma.201707035.
URL: https://onlinelibrary.wiley.com/doi/abs/10.1002/adma.201707035
DOI: 10.1002/adma.201707035

Yasa, O., Toshimitsu, Y., Michelis, M. Y., Jones, L. S., Filippi, M., Buchner, T., Katzschmann, R. K., May 2023. An Overview of Soft Robotics. Annual Review of Control, Robotics, and Autonomous Systems 6 (Volume 6, 2023), 1–29, publisher: Annual Reviews.
URL: https://www.annualreviews.org/content/journals/10.1146/annurev-control-062322-100607
DOI: 10.1146/annurev-control-062322-100607